AMERICAN SOCIETY FOR MICROBIOLOGY | Applied and Environmental Microbiology®

FOOD MICROBIOLOGY

Dual-Species Biofilms Formed by *Escherichia coli* and *Salmonella* Enhance Chlorine Tolerance

Zejia Lin,[a,b] Guoshu Wang,[a,b] Songshen Li,[a,b] Lehao Zhou,[a,b] Hongshun Yang[a,b]

[a]Department of Food Science & Technology, National University of Singapore, Singapore, Singapore
[b]National University of Singapore (Suzhou) Research Institute, Suzhou, Jiangsu, People's Republic of China

ABSTRACT In this research, mono- and dual-species biofilms of *Escherichia coli* (O45:H2 and O121:H19) and *Salmonella enterica* serovar Typhimurium formed on stainless-steel coupons were treated with 100 mg/L NaClO for 1 min. Confocal laser scanning microscopy (CLSM) was applied to investigate the spatial structural dynamics of mono- and dual-species biofilms, and nuclear magnetic resonance (NMR) spectroscopy was employed to further investigate their metabolic responses toward chlorine. CLSM results indicated that mixed-species biofilms (total biovolume, 148,000 to 167,000 μm^3) stimulated the growth of biomass 2 to 6 times that of single-species biofilms. Upon chlorine treatment, *E. coli* O45 and *S.* Typhimurium achieved less reduction ($P < 0.05$) when coexisting in mixed biofilms (0.70 and 1.17 log CFU/coupon reductions, respectively) compared with their corresponding single-species biofilms (1.97 and 2.01 log CFU/coupon reductions, respectively), while for *E. coli* O121, more reduction ($P < 0.05$) was achieved in a mixed biofilm (1.37 log CFU/coupon reductions) compared with its single-species biofilm (0.59 log CFU/coupon reductions). Moreover, NMR results suggested that the increase of putrescine (antioxidation regulator) and the decrease of glucose (enhanced glycolysis for energy replenishment) might contribute to the improved chlorine tolerance in mixed biofilms. Overall, dual-species biofilms promoted biofilm growth and their chlorine tolerance. This study improved our knowledge of the metabolic difference of single- and mixed-species biofilms of *E. coli* and *Salmonella* to chlorine sanitization and raised an urgency to investigate the effectiveness of common disinfectants against multispecies consortia.

IMPORTANCE Outbreaks of *Escherichia coli* and *Salmonella* in food might be associated with the cross-contamination of biofilms on food-contact surfaces. The knowledge of the sanitization of mono-species biofilm on the food-contact surface is well established, while mixed-species biofilm occurs more naturally, which could profoundly affect the efficacy of sanitizer. Therefore, this research aims to evaluate the efficacy of using chlorine against single- and dual-species biofilms of *E. coli* and *Salmonella* along with the underlying bacterial metabolic responses. The responses of a mixed biofilm of *E. coli* and *Salmonella* to chlorine sanitization were clarified, providing insights to develop a targeted and green sanitization strategy against specific pathogens by perturbing their most susceptible metabolism pathway without sanitizer residue.

KEYWORDS foodborne pathogen, metabolomics, NMR, CLSM, stainless steel, sodium hypochlorite

Shiga toxin-producing *Escherichia coli* (STEC) bacteria are severe foodborne pathogens that raise a public health risk as well as a substantial financial burden in the world. The most infamous STEC serotype linked with over 700,000 clinical illnesses per year in the United States is O157:H7, along with other serogroups (*E. coli* O111, O103, O145, O45, O121, and O26), which are also involved in many severe outbreaks, and are referred as the "big six" (1, 2). The symptoms of STEC infection range from slight diarrhea to serious hemolytic uremic syndrome (3, 4). Meanwhile, *Salmonella* is the second greatest source of bacterial foodborne

Editor Johanna Björkroth, University of Helsinki

Address correspondence to Hongshun Yang, fstynghs@nus.edu.sg.
The authors declare no conflict of interest.
Received 30 August 2022
Accepted 6 October 2022
Published 27 October 2022

disease in the United States, of which *Salmonella enterica* serovar Typhimurium is the most prevalent serotype that contributes to 11% of human gastroenteritis infections per year in the United States (5).

Both *Salmonella* and *E. coli* could adhere to various food-contact surfaces and produce biofilms which could function as a barrier against disinfectants and promote bacterial tolerance toward sanitizers compared with its planktonic cells (6–8). Our prior study showed that 100 mg/L chlorine sanitization for 1 min could not eradicate seven strains of *E. coli* biofilms on high-density polyethylene and stainless-steel (SS) surfaces. Among seven *E. coli* strains biofilms, O45 displayed the most perturbed metabolic status and pathways, while O121 displayed the least, demonstrating its low and high chlorine tolerance, respectively (9). Therefore, the establishment of foodborne pathogen biofilms on food-contact surfaces could pose a serious risk of cross-contamination to food, leading to serious food safety concerns.

Nearly all biofilms found in nature are made up of mixed species, and the intricate interactions within the biofilms have a substantial impact on the biofilm structure and biological activity (10). For instance, some studies found that the synergistic relationships in mixed-species biofilms may boost the growth of biofilm communities as well as tolerance against adverse environmental stress (11–13). On the other hand, a neutral or even competitive relationship was also reported in mixed-species biofilm communities (14). In addition, numerous foodborne pathogens species, such as *Salmonella*, *Listeria*, *Staphylococcus*, *Pseudomonas*, and *E. coli*, were proven to coexist in food processing facilities and grow biofilms together (15). However, current studies have focused mostly on the sanitization of single-species biofilms in the food processing environment, even though foodborne pathogen biofilms seem to be significantly skewed toward mixed-species communities, which might have a distinctive influence on sanitizer efficacy compared with single-species biofilms (16).

Hence, this research aimed to evaluate the effect of chlorine sanitizer on dual-species biofilms of *E. coli* and *S. Typhimurium*. *E. coli* O45 and O121 were chosen as the representative of a low-chlorine-tolerant strain and a high-chlorine-tolerant strain, respectively, according to our last research (9). The spatial structural dynamics of mono- and dual-species biofilms was deciphered by confocal laser scanning microscopy (CLSM). Moreover, nuclear magnetic resonance (NMR) spectroscopy was utilized for the detection of metabolic responses of survival cells upon chlorine to reveal the global picture of the bacterial defense mechanism. With the help of metabolome analysis, a guideline for disinfecting the food-contact surfaces could be provided by targeting the most perturbed pathway of pathogen biofilms via novel sanitizer or a combination with hurdle effects.

RESULTS AND DISCUSSION

Spatial analysis and quantification of single- and mixed-species biofilms. The characteristic CLSM scans of single-species biofilms of *E. coli* (O45 and O121) and *S.* Typhimurium as well as the mixed-species biofilms of O45 mixed with *S.* Typhimurium (O45mix) and O121 mixed with *S.* Typhimurium (O121mix) on SS surfaces are presented in Fig. 1, in which green dots represent the intact living cells and red dots represent the injured or dead cells. In accordance with the prior study, all species demonstrated the ability to build a biofilm (17, 18), especially denser green cells found in mixed biofilms. After chlorine treatment, the CLSM images revealed a large rise in the fraction of red cells on surfaces, suggesting that the membrane of most cells was damaged to a certain extent.

Figure 2 shows the biovolume as well as the maximum thickness of every single-species biofilm and their corresponding mixed biofilms. Under control groups (Fig. 2A), the total biovolume of monospecies biofilms ranged from 26,000 to 63,000 μm^3, while the total biovolume of O45mix and O121mix were significantly larger (167,000 and 148,000 μm^3, respectively), which suggested the mixed biofilms of O45mix and O121mix could substantially promote the biofilm development. Similarly, Rodríguez-Melcón et al. (19) also found that the biovolume of a *Salmonella* biofilm increased when mixed with *Staphylococcus aureus* or *Enterococcus faecium*. After chlorine treatment (Fig. 2B), a decrease in the total biovolume was observed among these five groups of biofilms, whereas the total biovolume of mixed biofilms was

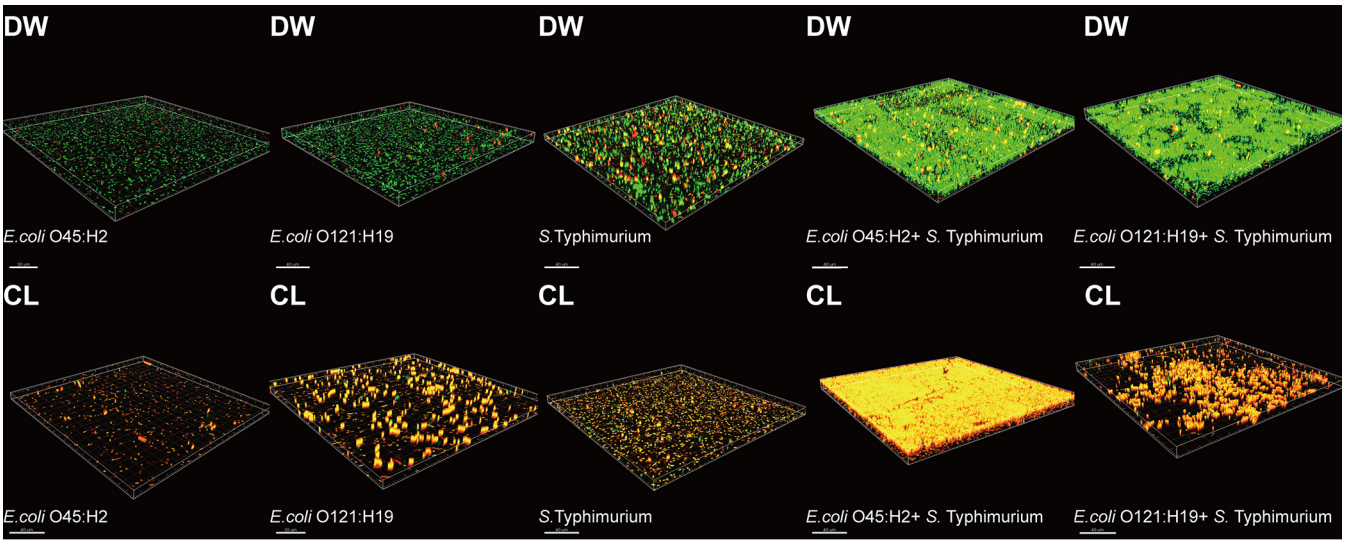

FIG 1 Three-dimensional confocal laser scanning microscopy (CLSM) images of *E. coli*, *S.* Typhimurium, and their dual-species biofilms with various treatments. DW, deionized water treatment; CL, 100-mg/L chlorine treatment; green dot, living cell; red dot, cell with compromised membrane.

still significantly higher than that of single biofilms. In terms of the maximum thickness of the biofilm (Fig. 2C), no distinguished difference was noticed among the five groups of biofilms either in the control or the treatment group. Only the thickness of the O45 biofilm was found to decrease markedly upon chlorine treatment, which implied its vulnerability toward chlorine sanitization, as revealed in our previous research (9).

The two-dimensional (2D) spatial organization of single- and dual-species biofilms with or without chlorine treatment is shown in Fig. 3. Interestingly, a unique pattern of biofilm spatial organization was found between *E. coli* and *S. T*yphimurium under all conditions. While *E. coli* grew biofilms with numerous cells evenly dispersed on the surfaces, *S.* Typhimurium grew extremely heterogeneous biofilms with scattered cell clusters. In addition, the two mixed-species biofilms also displayed obvious signs of cell clusters, which suggested *S.* Typhimurium dominated in the mixed biofilm.

Antimicrobial effect of chlorine on single- and mixed-species biofilms. The surviving population of each biofilm group with or without chlorine sanitization is shown in Fig. 4. On the one hand, under deionized water (DW) treatment, it is consistent with the biovolume result that the bacterial population of *E. coli* O45 (7.87 log CFU/coupon), O121 (7.95 log CFU/coupon), and *Salmonella* (8.71 and 8.56 log CFU/coupon, respectively) from the O45mix and O121mix was higher than that of their corresponding single-species biofilm (7.10, 7.08, and 6.83 log CFU/coupon, respectively).

Noticeably, compared with the *E. coli* population in mixed biofilms, the significantly higher population of *S.* Typhimurium in both mixed-species biofilms further evidenced the fact that *S.* Typhimurium could outgrow *E. coli* in mixed biofilms as discussed in "Spatial analysis and quantification of single- and mixed-species biofilms." Moreover, Chen et al. (20) and Wang et al. (21) also reported a dominance of *Salmonella* when forming a biofilm mixed with *E. coli*.

On the other hand, under chlorine treatment, O45, O121, and *S.* Typhimurium achieved 1.97, 0.59, and 2.01 log CFU/coupon reduction, respectively, while the reductions of *Salmonella* from O45mix and O121mix (1.17 and 1.50 log CFU/coupon, respectively; $P < 0.05$) were less than that of its single-species biofilm and the same as that for *E. coli* O45 from O45mix (0.7 log CFU/coupon reduction, $P < 0.05$). However, *E. coli* O121 from O121mix (1.37 log CFU/coupon reduction, $P < 0.05$) achieved more reduction than its single biofilm. In the Wang et al. (21) study, both *E. coli* O157:H7 strain FSIS11 and *S.* Typhimurium strain ST21843 displayed a markedly lower reduction upon 100 mg/L chlorine for 1 min when they coexisted in a mixed biofilm, whereas the mixed biofilm of O157 strain FSIS11 and *S.* Typhimurium ST12531 showed no enhanced tolerance. In addition, *Salmonella* strain 457-88 and *E. coli* O157:H7 strain USDA 5 were found to be more sensitive to sanitizer in a

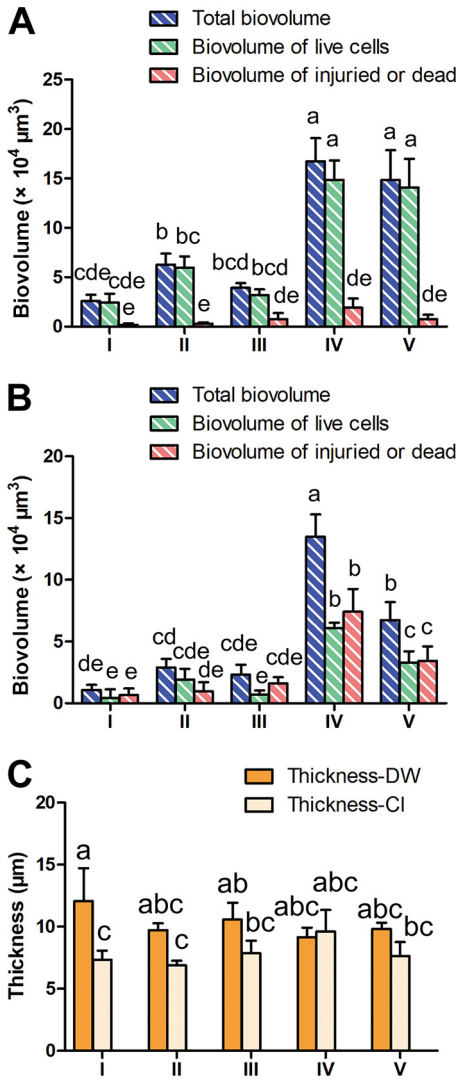

FIG 2 The biofilm profiles of *E. coli*, *S.* Typhimurium, and respective dual-species biofilms. Means ± standard deviations ($n = 3$) are used to present the data. The means with different letters indicate a significant difference ($P < 0.05$). I, O45:H2 (ATCC BAA-2193); II, O121:H19 (ATCC BAA-2219); III, *S.* Typhimurium (ATCC 14028); IV, mixed biofilm of *S.* Typhimurium and O45:H2; V, mixed biofilm of *S.* Typhimurium and O121:H19. (A) Biovolume of each biofilm upon deionized water treatment (DW). (B) Biovolume of each biofilm upon 100-mg/L chlorine treatment (Cl). (C) Maximum thickness of each biofilm upon DW and Cl.

mixed biofilm (20). Interestingly, in our research, both O45 and *S.* Typhimurium could benefit from an enhanced tolerance to chlorine sanitization in a mixed-species biofilm while O121 seemed to become less tolerant when presenting in a mixed biofilm. Therefore, it seems that the biofilm development as well as its bacterial susceptibility to a sanitizer was the result of reactions of both interspecies and interstrains within the biofilm community.

Metabolite profiles and multivariate analysis. The ^{1}H NMR spectra of a single-species biofilm of *E. coli* (O45 and O121) and *S.* Typhimurium along with their corresponding dual-species biofilm on SS surfaces are presented as Fig. S1 in the supplemental material. The ^{1}H and ^{13}C signals were assigned to corresponding metabolites (see Table S1 in the supplemental material), referring to the metabolite database (http://www.hmdb.ca/; http://www.bmrb.wisc.edu/metabolomics) and analysis of ^{1}H–^{13}C HSQC, as well as prior studies (22, 23). In total, 34 metabolites were identified in the biofilms of both mono- and dual-species biofilms, such as sugars, amino acids, nucleotides, organic acids, and other metabolites.

A principal-component analysis (PCA) was used to assess metabolite discrepancies and identify class variances to better understand the diversity among biofilm complexes of *E. coli*

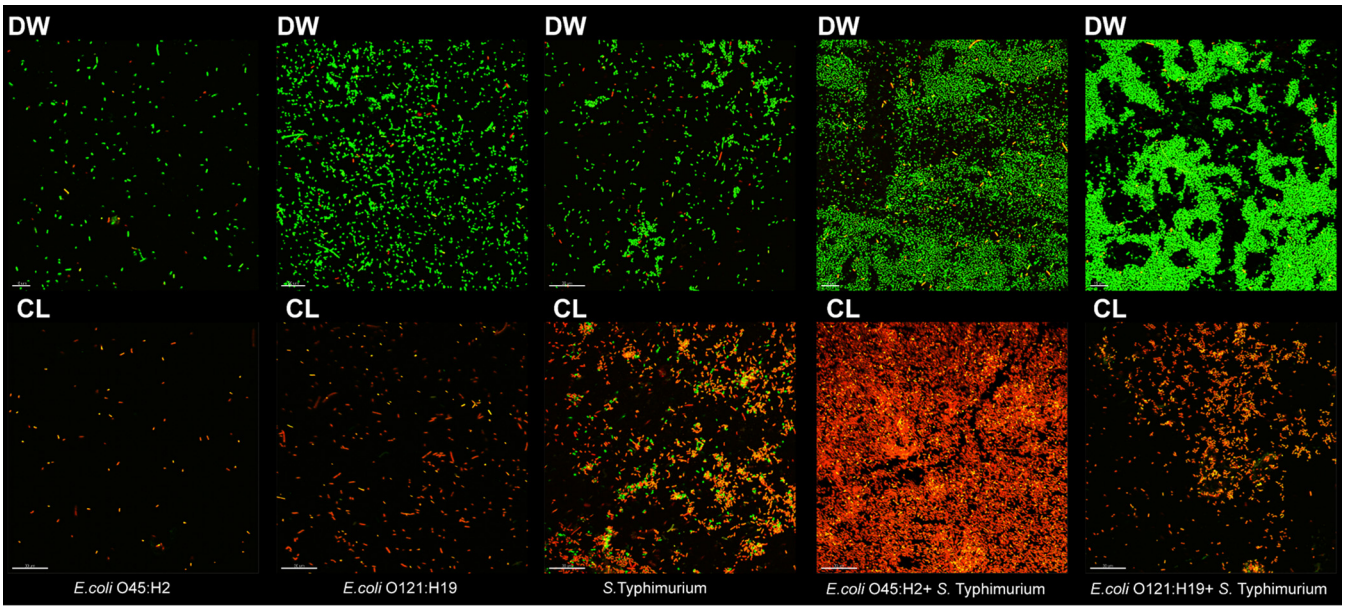

FIG 3 The slide views of mono-species biofilms of *E. coli* O45:H2, *E. coli* O121:H19, and *S.* Typhimurium and dual-species biofilms of *S.* Typhimurium and O45:H2, *S.* Typhimurium, and O121:H19 with various treatments. DW, deionized water treatment; CL, 100-mg/L chlorine treatment; green dot, living cell; red dot, cell with compromised membrane.

O45 and O121 and *S.* Typhimurium as well as their corresponding dual-species biofilms under various treatments. Based on quality parameters along with the three-dimensional (3D) score plots, the information of model quality and classification is illustrated in Fig. S2 in the supplemental material. For five various groups on coupons, the first six principal components (PCs) of DW-treated biofilms and the first five PCs of chlorine-treated biofilms explained 90.6% and 89.2% of the total data, respectively. The Q^2 value of these two PCA models were 0.78 (>0.50), which indicated a good predictability of these models (24). Upon DW treatment, the five groups of the biofilm community exhibited clear separation in the 3D score plot (Fig. S2A2), suggesting that the pattern of the metabolome could be distinguished among these five groups of biofilms. However, upon chlorine treatment, the two groups of mixed-species biofilm cannot be separated in the 3D score plot (Fig. S2B2), which meant their metabolic response to chlorine treatment was similar.

Orthogonal projection to latent structures-discriminant analysis (OPLS-DA) was performed on each biofilm group based on the detected metabolites between DW and chlorine

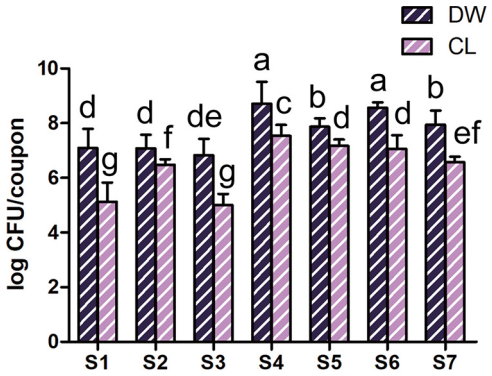

FIG 4 Effects of deionized water treatment (DW) and 100-mg/L chlorine treatment (CL) on the survival count of each biofilm on stainless steel coupons. Means ± standard deviations ($n = 3$) are used to present the data. The means with different letters indicate a significant difference ($P < 0.05$). S1, O45:H2 (ATCC BAA-2193); S2, O121:H19 (ATCC BAA-2219); S3, *S.* Typhimurium (ATCC 14028); S4, *S.* Typhimurium from mixed biofilm of *S.* Typhimurium and O45:H2; S5, O45:H2 from mixed biofilm of *S.* Typhimurium and O45:H2; S6, *S.* Typhimurium from mixed biofilm of *S.* Typhimurium and O121:H19; S7: O121:H19 from mixed biofilm of *S.* Typhimurium and O121:H19.

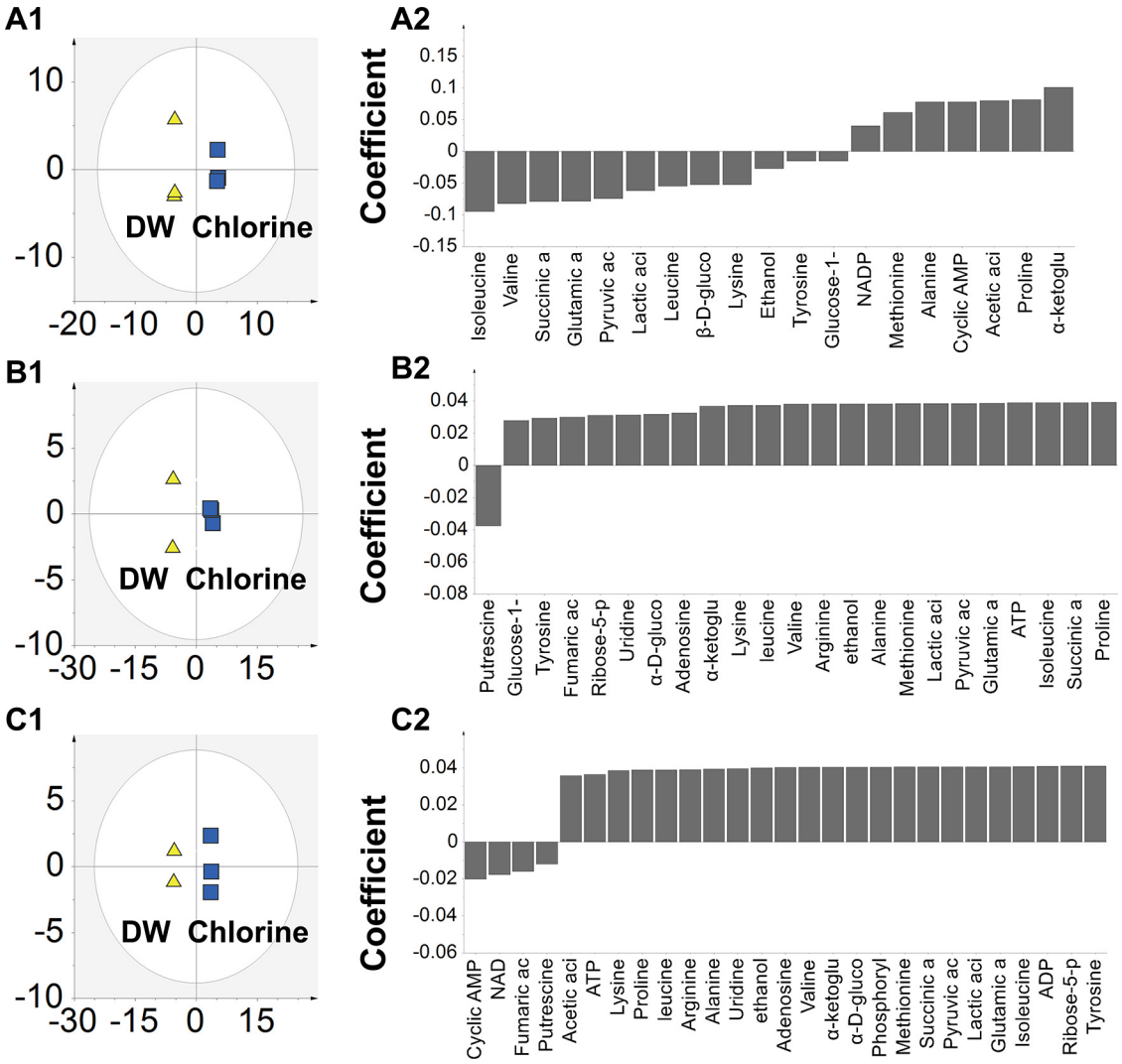

FIG 5 Orthogonal projections to latent structures-discriminant analysis (OPLS-DA) of three biofilm groups upon deionized water treatment (DW) and chlorine treatment. A1 to A2, score plot and coefficient plot of *S.* Typhimurium; B1 to B2, score plot and coefficient plot of mixed biofilm of *S.* Typhimurium and O45:H2; C1 to C2, score plot and coefficient plot of mixed biofilm of *S.* Typhimurium and O121:H19.

treatment, aiming to further pairwise groups for examination of the distinct variations in their metabolomes. Fig. 5 and Fig. S3 in the supplemental material present the OPLS-DA result as cross-validated score plots along with the coefficient plots. The values of R^2 and Q^2 (see Table S2 in the supplemental material) were all close to 1, implying the strong fitness and great predictability of these five biofilms groups (23). The score plots of these models (Fig. 5A1 to C1 and Fig. S3A1 to B1) showed clear separations between DW and chlorine treatment, suggesting that among all biofilm groups, a distinct metabolic alteration occurred upon chlorine sanitization. Moreover, coefficient plots of these models (Fig. 5A2 to C2 and Fig. S3A2 to B2) were utilized to filter the metabolites that are significant to the pairwise differentiation, of which upward and downward columns reflect higher and lower levels of metabolites, respectively, between DW and chlorine treatment.

Altered metabolites in single- and mixed-species biofilms upon chlorine treatment. The metabolites presented in coefficient plots were further filtered out (9), which are listed in Table 1 as significantly altered metabolites during chlorine sanitization. Overall, chlorine-induced stress led to various metabolic changes among different groups of biofilms. Specifically, the *S.* Typhimurium single-species biofilm displayed a general upward trend of metabolites. An elevated level of amino acids (e.g., Leu, Val, and Glu),

TABLE 1 Significantly affected metabolites in each biofilm groups after a 1-min chlorine[a] treatment

Metabolite category	Metabolite	Groups[b] showing significant increase (VIP > 1; FC >1.2; $P < 0.05$)	Groups[b] showing significant decrease (VIP > 1; FC < 0.83; $P < 0.05$)
Amino acids	Ala		O45mix, O121mix, O121[c]
	Arg		O45mix
	Glu	S	O45mix, O121mix, O45[c], O121[c]
	Ile		O45mix, O121mix, O45[c]
	Leu	S	O45mix, O45[c]
	Lys		O45mix, O121mix, O45[c], O121[c]
	Met		O45mix, O121mix, O45[c], O121[c]
	Pro		O45mix, O45[c], O121[c]
	Thr		O45[c]
	Tyr		O45mix, O121[c]
	Val	S	O45mix, O45[c], O121[c]
Nucleotide-related compounds	Adenosine		O45mix
	ATP	O121[c]	O45mix, O121mix
	Cyclic AMP	O121[c]	
	NAD		O45[c], O121[c]
	NADP		S
	Uridine		O45mix
Organic acids	Acetic acid		O45mix, S, O121[c]
	Fumaric acid		O45mix
	Lactic acid	S	O45mix, O121mix, O45[c]
	Pyruvic acid		O45mix, O121mix, O45[c]
	Succinic acid	S	O45mix, O121mix, O45[c]
	α-Ketoglutaric acid		O45mix, O121mix, S, O45[c], O121[c]
	γ-Aminobutyric acid		O45[c]
Alcohols	Ethanol		O45mix, O45[c], O121[c]
Sugar	Glucose-1-phosphate		O45mix
	Ribose-5-phosphate	O121[c]	O45mix, O45[c]
	α-D-Glucose		O45mix, O121mix, O45[c], O121[c]
	β-D-Glucose	O121[c]	
Others	Phosphorylcholine	O121[c]	O121mix, O45[c]
	Putrescine	O45mix	O45[c]

[a]100 mg/L NaClO.
[b]O45, *E. coli* O45:H2; O121, *E. coli* O121:H19; S, *S.* Typhimurium; O45mix, dual-species biofilms of O45:H2 mixed with *S.* Typhimurium; O121mix, dual-species biofilms of O121:H19 mixed with *S.* Typhimurium.
[c]Indicates these data are published in Lin et al. (9).

as well as organic acids (e.g., succinic acid and lactic acid) were noticed, whereas the content of NADP and α-ketoglutaric acid were found to decline.

Consistent with our previous finding (9), a depletion of a range of metabolites was detected in the O45 single-species biofilm after chlorine treatment, including amino acids (e.g., Val, Pro, Ala, Met, Leu, Lys Ile, and Thr), sugars (e.g., ribose-5-phosphate and α-D-glucose), organic acids (e.g., α-ketoglutaric acid, pyruvic acid, lactic acid, and γ-aminobutyric acid [GABA]), and nucleotide-related compounds (NAD). Consistent results were also found in a O121 single biofilm; fewer amino acids (e.g., Met, Glu, Ala, and Pro) were reported to decrease and elevated levels of sugars (ribose-5-phosphate and β-D-glucose), as well as nucleotide-related compounds (cyclic AMP and ATP), were also noticed. Besides, metabolites (putrescine and phosphorylcholine) associated with bacterial defense mechanisms displayed upward trends (25).

O45mix demonstrated a unique metabolic pattern with a significant increase in putrescine content compared with the single-species biofilms of O45 and *S.* Typhimurium. In addition, organic acids (e.g., α-ketoglutaric acid, lactic acid, and acetic acid) were found to decrease in O45mix, which is opposite the upward trend in the *S.* Typhimurium single-species biofilm. Otherwise, the depletion of amino acids (e.g., Met, Tyr, Ala, Glu, and Leu) and sugars (e.g., ribose-5-phosphate and α-D-glucose), as well as nucleotide-related compounds (e.g., adenosine and ATP), was comparable to that of the O45 single biofilm.

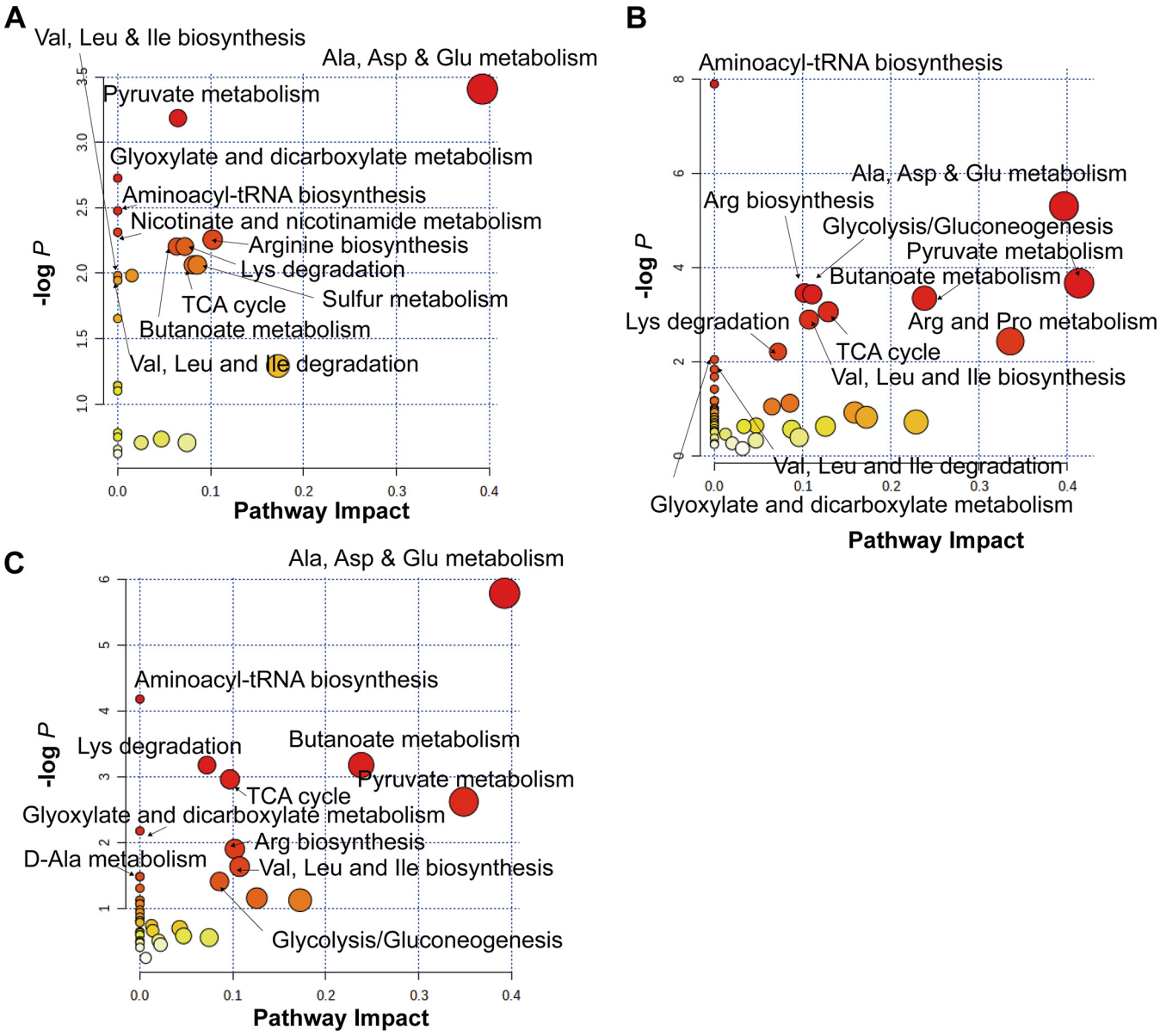

FIG 6 Alteration of metabolic pathways induced by chlorine stress in three groups of biofilms on stainless steel (SS) surfaces. (A) *S.* Typhimurium. (B) Mixed biofilm of *S.* Typhimurium and O45:H2. (C) Mixed biofilm of *S.* Typhimurium and O121:H19. Bullet colors ranging from yellow to red indicate the metabolites with elevated levels of significance.

O121mix also displayed a distinctive pattern of metabolic response to chlorine stress compared with its corresponding single-species biofilms. An upward trend of amino acids (e.g., Met, Ala, Glu, Ile, and Lys) and a downward trend of organic acids (e.g., α-ketoglutaric acid, pyruvic acid, lactic acid, and succinic acid) were found in O121mix, whereas the opposite trend occurred in the *S.* Typhimurium single biofilm. Moreover, ATP and phosphorylcholine were downregulated in O121mix but upregulated in the O121 single biofilm.

Altered metabolic pathway in single- and mixed-species biofilms upon chlorine treatment. To further investigate the alterations in the metabolic pathway of the biofilm groups after chlorine sanitization, MetaboAnalyst 5.0 was utilized to identify the substantially changed pathways in each biofilm group, and those pathways with a *P* value of <0.05 were deemed crucial to the sanitizing process. They are described in Table S3 in the supplemental material and are shown in Fig. 6 and Fig. S4 in the supplemental material as circles, where the bullet colors within the pathway, varying from yellow to red, indicated the metabolites in the data set with increasing significance. Multiple pathways were universally

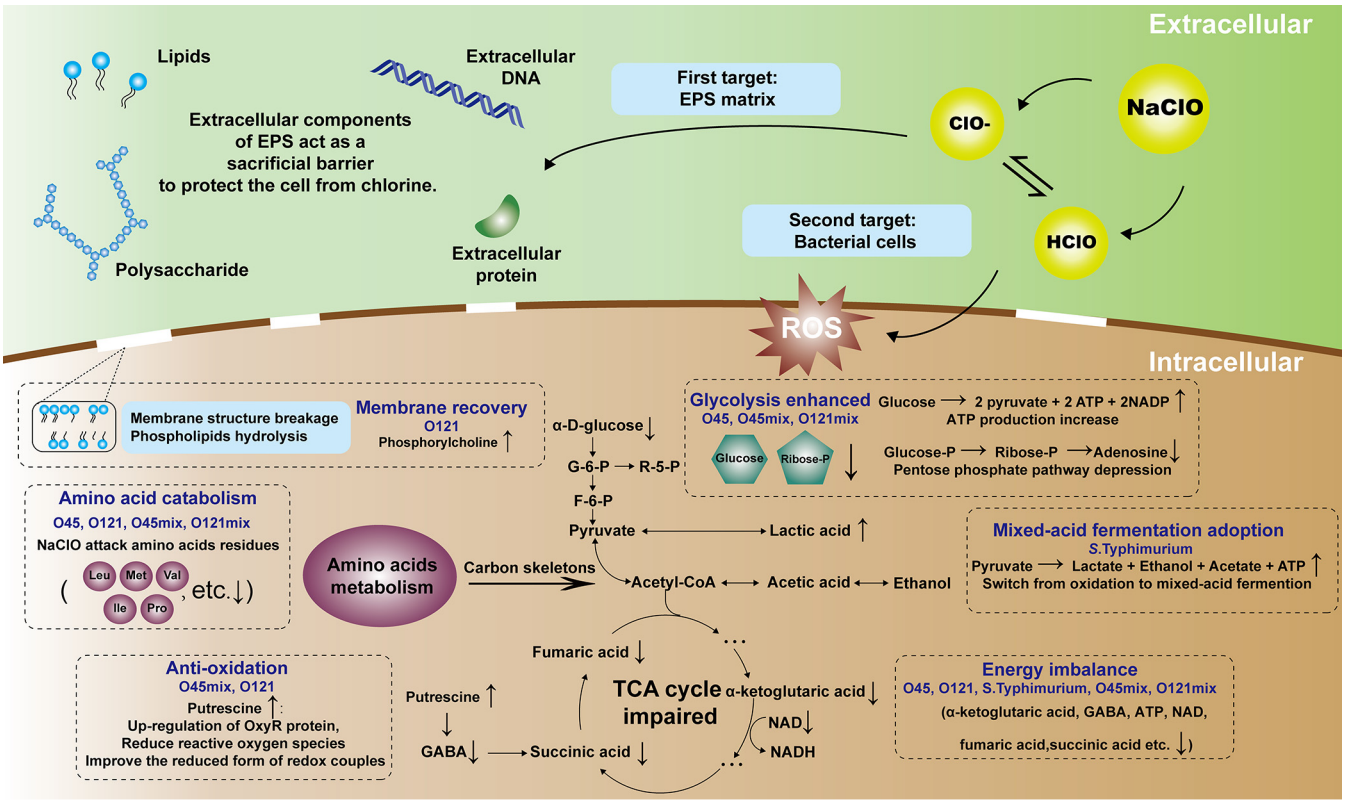

FIG 7 Proposed metabolic responses associated with chlorine tolerance of mono-species biofilms of *E. coli* O45:H2 (O45), O121:H19 (O121), and *S.* Typhimurium and dual-species biofilms of *S.* Typhimurium and O45:H2 (O45mix) and *S.* Typhimurium and O121:H19 (O121mix).

interrupted. Specifically, aminoacyl-tRNA biosynthesis, a process in amino acid metabolism responsible for accurate matching of amino acid with its corresponding tRNA, Ala, Asp, and Glu metabolism, a process of amino acid conversion, and arginine biosynthesis were drastically changed in all five groups of biofilms. Moreover, the citrate cycle (trichloroacetic acid [TCA] cycle) and glycolysis/gluconeogenesis as well as Val, Leu, and Ile biosynthesis were all dramatically altered in four groups (O45, *S.* Typhimurium, O45mix, and O121mix; O45, O121, O45mix, and O121mix; O45, *S.* Typhimurium, O45mix, and O121mix).

Based on the Kyoto Encyclopedia of Genes and Genomes (KEGG) database, Fig. 7 depicts a schematic model exhibiting the metabolic responses of five groups of biofilms during chlorine exposure, with rationales for the chlorine tolerance of each group.

On the one hand, in the extracellular environment, the composition of extracellular polymeric substances (EPS) includes polysaccharides, which are influential constituents of EPS supporting the structure of the biofilm, along with other substances, such as extracellular DNA, proteins, and lipids (26). These biomolecules in EPS act as the first target, protecting the bacterial cell from chlorine exposure during the sanitization process (27).

On the other hand, based on the significant change of amino acids detected inside the cells, the amino acid metabolism was the most affected pathway in all biofilm groups, as indicated by prior research that in a wide variety of bacteria, amino acids biosynthesis is extremely sensitive to environmental stress, such as oxidation, high acidity, and heat (1). For all biofilm groups except the *S.* Typhimurium single biofilm, the amino acid depletion might be linked to certain amino acid residues on extracellular proteins, which could be targeted and damaged by the external oxides (27). Moreover, sulfurous and aromatic amino acids (e.g., Met, Cys, Tyr, and Phe) are more vulnerable to oxidative stress (28). However, the increasing level of Leu, Val, and Glu in the single-species biofilm of *S.* Typhimurium might imply an initiation of certain protein synthesis as an adaptation to chlorine-induced stress, as Lushchak (29) reported that HClO may trigger *oxyR* and *soxRS* expression, resulting in the

formation of OxyR, SoxS, and SoxR proteins, which operate as an antioxidant mechanism and defend the cell against superoxide anion and hydrogen peroxide assault.

Following amino acid metabolism, the carbon material is sent to the TCA cycle for energy generation (30). After the chlorine sanitization, all biofilm groups showed considerable depletion of TCA-associated metabolites (e.g., GABA, α-ketoglutaric acid, fumaric acid, succinic acid, ATP, and NAD), indicating that the TCA cycle was impaired to various degrees (31). As a result, the biofilm groups were urged to take steps to compensate for the energy imbalance during chlorine sanitizations.

Under adverse conditions, bacteria could enhance glycolysis for energy supplements. Three biofilm groups (O45, O45mix, and O121mix) simultaneously showed a considerable drop in glucose, indicating that they were speeding up glycolysis for energy production. Zhang et al. (32) reported that the expression of glycolysis genes, such as *glk*, *pgk*, *pykF*, and *pgi*, which encode hexokinase, phosphoglycerate kinase, pyruvate kinase I, and glucose-6-phosphate isomerase, respectively, was significantly activated in a hostile environment, demonstrating the importance of the glycolysis pathway for energy replenishment. In addition, the pentose phosphate pathway (PPP), which shunts glycolysis by utilizing the glucose-6-phosphate to make fructose-6-phosphate (33), was also impacted, as demonstrated by the notable drop in ribose-5-phosphate in O45 and O45mix. Since PPP does not produce ATP, its depletion would funnel all accessible glucose into the pathway of glycolysis, allowing microorganisms to restore their high energy demand constantly.

Unsurprisingly, the level of ATP and ribose-5-phosphate decreased in O121mix but increased in the O121 single biofilm, indicating less energy supply in O121mix than O121 single biofilm, which once again evidenced that a higher reduction of O121 was achieved in a mixed biofilm as discussed in "Antimicrobial effect of chlorine on single- and mixed-species biofilms." Although no sugar depletion was observed in the *S.* Typhimurium single biofilm, the boost of lactic acid suggested that the microorganisms might convert from oxidation to mixed-acid fermentation for energy supply (1). However, since anaerobic respiration is less energy efficient than aerobic respiration (34), less available energy for *S.* Typhimurium in a single biofilm might potentially explain its higher reduction upon chlorine in a single biofilm than in the mixed biofilms.

The variance of chlorine tolerance between single-and mixed-species biofilms might be associated with putrescine, an antioxidative stress regulator. Prior study has shown that putrescine can promote *oxyR* gene expression in *E. coli* cells when facing NaClO (35). OxyR proteins are important components of the antioxidant system since they control various oxidation-inducible activity expression (e.g., *ahpCF*, *catG*, and *gorA*) (36). Therefore, the boosting putrescine found in O45mix may indirectly aid the cell in reducing reactive oxygen species and improving the reduced form of redox couples, which contribute to the enhanced chlorine tolerance compared with its corresponding single-species biofilms. However, the rise of putrescine was only found in O121 single biofilm, but not found in O121mix and same happened to the phosphorylcholine, an essential precursor of membrane phospholipid, and critical for membrane integrity maintenance (37). Hence, a low level of these two metabolites might collectively lead to the weaken chlorine tolerance in O121mix compared with that in a O121 single biofilm.

Conclusion. Mono- and dual-species biofilms of *E. coli* O45 and O121 and *S.* Typhimurium on SS surfaces were examined against chlorine sanitization. CLSM images of each biofilm group revealed that mixed biofilms of *E. coli* and *S.* Typhimurium could promote biomass growth, as the greatest biovolume of biofilm was recorded in O45mix and O121mix. Moreover, bacterial enumeration results proved that the chlorine tolerance was improved in O45 and *S.* Typhimurium but weakened in O121 when they existed in mixed biofilms. The NMR analysis further illustrated their mechanism toward chlorine at the metabolome level. Overall, *Salmonella* switched from anaerobic to aerobic respiration in a mixed biofilm upon chlorine treatment to obtain more energy. O45mix acquired a stronger chlorine tolerance than its corresponding single biofilms with an antioxidation mechanism, while O121mix debilitated its chlorine tolerance via the deactivation of the defense system as well as low energy supply. The findings in this study offer insights to better understand the mechanism

of mono- and dual-species biofilms against chlorine, which benefits alterations to sanitization and artificially activates the most critical metabolic pathways to boost antibacterial efficacy.

MATERIALS AND METHODS

Bacterial strains and culture conditions. *E. coli* O45:H2 (ATCC BAA-2193) and O121:H19 (ATCC BAA-2219) and *S.* Typhimurium (ATCC 14028) were utilized in this research. Each strain (100 μL) was activated by inoculation into a 50-mL tube with 10 mL of tryptone soya broth (TSB; Sigma-Aldrich, St. Louis, MO) at 37°C for 24 h. *S.* Typhimurium was further adapted to nalidixic acid (NA; 100 μg/mL) based on a prior procedure (38). Before use, strains were inoculated into TSB (40 mL) overnight at 37°C, after which the cell pellets were collected by centrifugation at 3,600 $\times$ *g* for 10 min at 23°C, then washed twice with 10 mL peptone water (PW; 0.1%), and finally resuspended in 10 mL PW for biofilm inoculation.

Mono- and dual-species biofilm inoculation on food-contact surfaces. The procedure of single- and mixed-species biofilm formation was adopted from previous research, with certain modifications (39–41). Specifically, for single-species biofilms of *E. coli* O45 and O121, and *S.* Typhimurium, 200 μL of each strain suspension was added into 20 mL of low-concentration TSB (LC-TSB; 1:10) with a piece of sterile stainless steel (SS) coupon (type, 304; 5 cm $\times$ 2 cm). For mixed-species biofilms of O45 with *S.* Typhimurium and O121 with *S.* Typhimurium, *E. coli* and *S.* Typhimurium suspensions were mixed well at a ratio of 1:1, of which 200 μL was used to inoculate on coupons with 20 mL LC-TSB. Each coupon was incubated at 25°C for 4 h to promote cell attachment, following which the coupons were carefully washed in 10 mL PW to loosely dislodge attached cells and then were transferred to fresh 10 mL LC-TSB at 25°C. Upon 48 h of incubation, the LC-TSB was discarded, and the SS coupon was then moved to fresh LC-TSB at 25°C for another 24 h. Upon the incubations described above, the SS coupon was carefully rinsed twice with 5 mL PW to dislodge any attached cells before being stored in a biosafety cabinet for 2 h to dry.

Biofilm sanitization of biofilms on the SS surfaces. Ten pieces of inoculated SS coupons were submerged in a sterile 500-mL container with a 100-mL NaClO solution (100 mg/L), which was acquired by diluting chlorine bleach (5% NaClO; Fairprice, Singapore) before use. Based on previous research (42, 43), we chose a 1-min exposure duration for the NaClO solution to better observe sanitization tolerance and any possible elevated bacterial population in single- and dual-species biofilms. Besides, the same procedures were followed for the control group, utilizing 100 mL of sterile deionized water (DW). After 1 min of treatment, 10 pieces of treated SS coupons were submerged in 100-mL Dey-Engley solution (1 min) to neutralize sanitizers before being put in a biosafety cabinet to dry.

CLSM and image analysis. CLSM analysis was performed based on a previously described approach with adjustments (44) to visualize the structure of mono- and dual-species biofilms following various treatments. Live/Dead BacLight viability kit L-7007 (Molecular Probes, Eugene, USA) was used to stain the biofilms on SS coupons. After a 15-min incubation period in the dark, the coupons were analyzed instantly using an inverted Fluoview FV 1000 laser scanning confocal microscope (Olympus, Tokyo, Japan) equipped with a 60$\times$ water-immersion lens objective and argon lasers of 473 and 559 nm. For each biofilm group, three stacks of horizontal plane pictures (1,024 $\times$ 1,024 pixels equivalent to 211 $\times$ 211 μm) with a z-step of 0.58 μm were taken at three distinct sites on the coupon. The "3D review" and "Slice" tools of the IMARIS 9.0 software (Bitplane, Switzerland) were used to rebuild three- and two-dimensional projections of each biofilm structure, respectively. Quantitative characteristics of the biofilms, such as biovolume (μm^3) and maximum thickness (μm) were quantified by BiofilmQ (45) (https://drescherlab.org/data/biofilmQ) and COMSTAT (http://www.comstat.dk), respectively. The biovolume indicated the total volume of bacteria in the observation area of 44,521 μm^2, and it offered a biomass estimation of the biofilm (46).

Bacteria enumeration of mono- and dual-species biofilms. For single-species biofilms, coupons acquired in "Biofilm sanitization of biofilms on the SS surfaces" were transferred to a 50-mL tube containing 20 mL PW and 2-g glass beads (4 mm), and the attached bacteria were removed from the coupon by vortexing for 1 min. The detached cell suspension was serially diluted by PW, of which 100 μL was spread onto tryptic soy agar (TSA; Sigma-Aldrich, St. Louis, MO) and incubated at 37°C for 24 h. The bacterial counting results were presented as CFU per coupon. For mixed-species biofilms, the CFU of *S.* Typhimurium in dual-species biofilms was directly determined by the total CFU in TSA with NA (TSA-NA), while the CFU of *E. coli* in mixed-species biofilms was calculated as the difference between the total CFU in TSA without NA and the CFU of *S.* Typhimurium in TSA-NA.

Extraction of biofilm metabolites. The metabolomics investigation was carried out on each biofilm group, adopting a reported method (40) with some modifications. To obtain enough metabolites for NMR analysis, 10 pieces of SS coupons of each biofilm group were used to make the detached cell suspension discussed in "Bacteria enumeration of mono- and dual-species biofilms," after which they were subject to centrifugation (16,000 $\times$ *g*, 10 min, and 4°C) and resuspended in fresh TSB (20 mL) for 6 h at 37°C. The concentrated bacterial suspension was centrifuged again (16,000 $\times$ *g*, 10 min, and 4°C), washed twice by PW (5 mL), and resuspended in ice-cold methanol-d4 (1 mL). Three freeze-thaw cycles using liquid nitrogen were applied to break the membrane structure, and then metabolites were extracted overnight at $-$20°C after centrifugation (12,000 $\times$ *g*, 20 min, 4°C). The obtained supernatant was spiked with 1 mM trimethylsilyl propanoic acid (TSP) and then prepared for the NMR analysis.

NMR testing and spectral analysis. The NMR test was carried out using a triple inverse gradient probe on an NMR spectrometer (Bruker DRX-500). The NOESY pulse sequence was used to collect data from the ^{1}H spectrum. In addition, the spectra of all samples were analyzed with a 1-Hz line widening factor before the Fourier transform. At 298 K, 2D ^{1}H–^{13}C heteronuclear single quantum coherence spectroscopy of each sample was obtained for metabolite identification and quantification. The ^{1}H signal was captured on the F2 channel of spectral (10-ppm width), and the ^{13}C signal was captured on the F1 channel of spectral (175-ppm width).

Based on the Mahmud et al. (47) method with modifications, the ^{1}H spectrum data were adjusted for baseline and phase automatically; then peaks were normalized to sum intensities, water area (4.90 to 5.00 ppm) was cut off, and lastly data were binned into baskets with a 0.02-ppm integral width, using Mnova software (Mestreab, Spain).

Principal-component analysis (PCA) was performed on the binned data to show the differences among various biofilm groups as well as the orthogonal projection to latent structures-discriminant analysis (OPLS-DA) for differences between the control and treatment groups, using SIMCA 14.0 (Umetrics, Sweden) (48). To filter out substantially changed metabolites during chlorine treatment, the results from the OPLS-DA data were investigated utilizing the fold change (FC), the variable importance in projection (VIP), and the related *P* values in each pairwise comparison. Lastly, referring to the Kyoto Encyclopedia of Genes and Genomes (KEGG) database (https://www.genome.jp/kegg/pathway.html), filtered metabolites were subject to enrichment pathway analysis, using MetaboAnalyst 5.0 (https://www.metaboanalyst.ca/).

Statistical analysis. Each assay was carried out individually in triplicate. Duncan's multiple range test was applied to conduct the one-way analysis of variance (ANOVA) ($P < 0.05$) in SPSS Statistics software (IBM Corp., Armonk, NY) for mean comparisons between different treatment groups.

SUPPLEMENTAL MATERIAL

Supplemental material is available online only.

SUPPLEMENTAL FILE 1, PDF file, 0.8 MB.

ACKNOWLEDGMENTS

This research was financed by the Singapore Ministry of Education Academic Research Fund Tier 1 (A-8000469-00-00) and an industry grant supported by Shanghai Congwu Industrial Co., Ltd. (A-0004846-00-00).

We declare no conflict of interest.

REFERENCES

1. Wang Y, Zhou D, Yang H. 2022. Metabolic responses of "big six" *Escherichia coli* in wheat flour to thermal treatment revealed by nuclear magnetic resonance spectroscopy. Applied Environ Microbiol 88:e00098-22. https://doi.org/10.1128/aem.00098-22.
2. Browne AS, Midwinter AC, Withers H, Cookson AL, Biggs PJ, Marshall JC, Benschop J, Hathaway S, Haack NA, Akhter RN, French NP. 2018. Molecular epidemiology of shiga toxin-producing *Escherichia coli* (STEC) on New Zealand dairy farms: application of a culture-independent assay and whole-genome sequencing. Appl Environ Microbiol 84:e00481-18. https://doi.org/10.1128/AEM.00481-18.
3. Wang W, Sang Y, Liu J, Liang X, Guo S, Liu L, Yuan Q, Xing C, Pan S, Wang L. 2021. Identification of novel monoclonal antibodies targeting the outer membrane protein C and lipopolysaccharides for *Escherichia coli* O157:H7 detection. J Appl Microbiol 130:1245–1258. https://doi.org/10.1111/jam.14849.
4. Luu P, Chhetri VS, Janes ME, King JM, Adhikari A. 2020. Effectiveness of aqueous chlorine dioxide in minimizing food safety risk associated with *Salmonella*, *E. coli* O157: H7, and *Listeria monocytogenes* on sweet potatoes. Foods 9:1259. https://doi.org/10.3390/foods9091259.
5. Park M-Y, Kang D-H. 2021. Antibacterial activity of caffeic acid combined with UV-A light against *Escherichia coli* O157:H7, *Salmonella enterica* serovar Typhimurium, and *Listeria monocytogenes*. Appl Environ Microbiol 87:e00631-21. https://doi.org/10.1128/AEM.00631-21.
6. von Hertwig AM, Prestes FS, Nascimento MS. 2022. Biofilm formation and resistance to sanitizers by *Salmonella* spp. Isolated from the peanut supply chain. Food Res Int 152:110882. https://doi.org/10.1016/j.foodres.2021.110882.
7. Zhao L, Zhang Y, Yang H. 2017. Efficacy of low concentration neutralised electrolysed water and ultrasound combination for inactivating *Escherichia coli* ATCC 25922, *Pichia pastoris* GS115 and *Aureobasidium pullulans* 2012 on stainless steel coupons. Food Control 73:889–899. https://doi.org/10.1016/j.foodcont.2016.09.041.
8. Tan J, Yi J, Yang X, Lee H, Nitin N, Karwe M. 2022. Distribution of chlorine sanitizer in a flume tank: numerical predictions and experimental validation. Lwt 155:112888. https://doi.org/10.1016/j.lwt.2021.112888.
9. Lin Z, Chen T, Zhou L, Yang H. 2022. Effect of chlorine sanitizer on metabolic responses of *Escherichia coli* biofilms "big six" during cross-contamination from abiotic surface to sponge cake. Food Res Int 157:111361. https://doi.org/10.1016/j.foodres.2022.111361.
10. Wang N, Jin Y, He G, Yuan L. 2021. Development of multi-species biofilm formed by thermophilic bacteria on stainless steel immerged in skimmed milk. Food Res Int 150:110754. https://doi.org/10.1016/j.foodres.2021.110754.
11. Cheng Y, Zhang S, Zhang C, Mi X, Zhang W, Wang L, Liu W, Jiang Y. 2022. *Escherichia coli* O157: H7 is challenged by the presence of *Pseudomonas*, but successfully co-existed in dual-species microbial communities. Food Microbiol 106:104034. https://doi.org/10.1016/j.fm.2022.104034.
12. Schwering M, Song J, Louie M, Turner RJ, Ceri H. 2013. Multi-species biofilms defined from drinking water microorganisms provide increased protection against chlorine disinfection. Biofouling 29:917–928. https://doi.org/10.1080/08927014.2013.816298.
13. Tan J, Karwe MV. 2021. Inactivation and removal of *Enterobacter aerogenes* biofilm in a model piping system using plasma-activated water (PAW). Innov Food Sci Emerg Technol 69:102664. https://doi.org/10.1016/j.ifset.2021.102664.
14. Milho C, Silva MD, Alves D, Oliveira H, Sousa C, Pastrana LM, Azeredo J, Sillankorva S. 2019. *Escherichia coli* and *Salmonella Enteritidis* dual-species biofilms: interspecies interactions and antibiofilm efficacy of phages. Sci Rep 9:18183. https://doi.org/10.1038/s41598-019-54847-y.
15. Culotti A, Packman AI. 2014. Pseudomonas aeruginosa promotes *Escherichia coli* biofilm formation in nutrient-limited medium. PLoS One 9:e107186. https://doi.org/10.1371/journal.pone.0107186.
16. Kim U, Kim J-H, Oh S-W. 2022. Review of multi-species biofilm formation from foodborne pathogens: multi-species biofilms and removal methodology. Crit Rev Food Sci Nutr 62:5783–5793.
17. Jiang W, Waldman C, Li K, Jaczynski J, Shen C. 2021. Survival of *Salmonella* and the surrogate *Enterococcus faecium* in cooking of moisture enhanced reconstructed comminuted chicken patties by double pan-broiling. Poultry Science 100:101171. https://doi.org/10.1016/j.psj.2021.101171.
18. Canakapalli SS, Sheng L, Wang L. 2022. Survival of common foodborne pathogens on dates, sundried tomatoes, and dried pluots at refrigerated and ambient temperatures. Lwt 154:112632. https://doi.org/10.1016/j.lwt.2021.112632.
19. Rodríguez-Melcón C, Alonso-Hernando A, Riesco-Peláez F, García-Fernández C, Alonso-Calleja C, Capita R. 2021. Biovolume and spatial distribution of foodborne Gram-negative and Gram-positive pathogenic bacteria in mono-and dual-species biofilms. Food Microbiol 94:103616. https://doi.org/10.1016/j.fm.2020.103616.
20. Chen D, Zhao T, Doyle MP. 2015. Single- and mixed-species biofilm formation by *Escherichia coli* O157:H7 and *Salmonella*, and their sensitivity to levulinic acid plus sodium dodecyl sulfate. Food Control 57:48–53. https://doi.org/10.1016/j.foodcont.2015.04.006.
21. Wang R, Kalchayanand N, Schmidt JW, Harhay DM. 2013. Mixed biofilm formation by Shiga toxin–producing *Escherichia coli* and *Salmonella enterica* serovar Typhimurium enhanced bacterial resistance to sanitization due

to extracellular polymeric substances. J Food Prot 76:1513–1522. https://doi.org/10.4315/0362-028X.JFP-13-077.
22. Guo C, He Y, Wang Y, Yang H. 2022. NMR-based metabolomic investigation on antimicrobial mechanism of *Salmonella* on cucumber slices treated with organic acids. Food Control 137:108973. https://doi.org/10.1016/j.foodcont.2022.108973.
23. Chen L, Zhao X, Wu J, Liu Q, Pang X, Yang H. 2020. Metabolic characterisation of eight *Escherichia coli* strains including "big six" and acidic responses of selected strains revealed by NMR spectroscopy. Food Microbiol 88:103399. https://doi.org/10.1016/j.fm.2019.103399.
24. He Y, Zhao X, Chen L, Zhao L, Yang H. 2021. Effect of electrolysed water generated by sodium chloride combined with sodium bicarbonate solution against *Listeria innocua* in broth and on shrimp. Food Control 127:108134. https://doi.org/10.1016/j.foodcont.2021.108134.
25. Zhao L, Zhao MY, Phey CP, Yang H. 2019. Efficacy of low concentration acidic electrolysed water and levulinic acid combination on fresh organic lettuce (Lactuca sativa Var. Crispa L.) and its antimicrobial mechanism. Food Control 101:241–250. https://doi.org/10.1016/j.foodcont.2019.02.039.
26. Koo H, Allan RN, Howlin RP, Stoodley P, Hall-Stoodley L. 2017. Targeting microbial biofilms: current and prospective therapeutic strategies. Nat Rev Microbiol 15:740–755. https://doi.org/10.1038/nrmicro.2017.99.
27. Yu H, Liu Y, Li L, Guo Y, Xie Y, Cheng Y, Yao W. 2020. Ultrasound-involved emerging strategies for controlling foodborne microbial biofilms. Trends Food Sci Technol 96:91–101. https://doi.org/10.1016/j.tifs.2019.12.010.
28. Yang L, Mih N, Anand A, Park JH, Tan J, Yurkovich JT, Monk JM, Lloyd CJ, Sandberg TE, Seo SW, Kim D, Sastry AV, Phaneuf P, Gao Y, Broddrick JT, Chen K, Heckmann D, Szubin R, Hefner Y, Feist AM, Palsson BO. 2019. Cellular responses to reactive oxygen species are predicted from molecular mechanisms. Proc Natl Acad Sci U S A 116:14368–14373. https://doi.org/10.1073/pnas.1905039116.
29. Lushchak VI. 2011. Adaptive response to oxidative stress: bacteria, fungi, plants and animals. Comp Biochem Physiol C Toxicol Pharmacol 153:175–190. https://doi.org/10.1016/j.cbpc.2010.10.004.
30. Lungu B, Ricke S, Johnson M. 2009. Growth, survival, proliferation and pathogenesis of *Listeria monocytogenes* under low oxygen or anaerobic conditions: a review. Anaerobe 15:7–17. https://doi.org/10.1016/j.anaerobe.2008.08.001.
31. Koebmann BJ, Westerhoff HV, Snoep JL, Nilsson D, Jensen PR. 2002. The glycolytic flux in *Escherichia coli* is controlled by the demand for ATP. J Bacteriol 184:3909–3916. https://doi.org/10.1128/JB.184.14.3909-3916.2002.
32. Zhang W, Chen X, Sun W, Nie T, Quanquin N, Sun Y. 2020. *Escherichia coli* increases its ATP concentration in weakly acidic environments principally through the glycolytic pathway. Genes 11:991. https://doi.org/10.3390/genes11090991.
33. Ge T, Yang J, Zhou S, Wang Y, Li Y, Tong X. 2020. The role of the pentose phosphate pathway in diabetes and cancer. Front Endocrinol (Lausanne) 11:365. https://doi.org/10.3389/fendo.2020.00365.
34. Ye Y, Zhang L, Hao F, Zhang J, Wang Y, Tang H. 2012. Global metabolomic responses of *Escherichia coli* to heat stress. J Proteome Res 11:2559–2566. https://doi.org/10.1021/pr3000128.
35. Tkachenko A, Nesterova L, Pshenichnov M. 2001. The role of the natural polyamine putrescine in defense against oxidative stress in *Escherichia coli*. Arch Microbiol 176:155–157. https://doi.org/10.1007/s002030100301.
36. Liu Q, Chen L, Laserna AKC, He Y, Feng X, Yang H. 2020. Synergistic action of electrolyzed water and mild heat for enhanced microbial inactivation of *Escherichia coli* O157:H7 revealed by metabolomics analysis. Food Control 110:107026. https://doi.org/10.1016/j.foodcont.2019.107026.
37. Geiger O, López-Lara IM, Sohlenkamp C. 2013. Phosphatidylcholine biosynthesis and function in bacteria. Biochim Biophys Acta 1831:503–513. https://doi.org/10.1016/j.bbalip.2012.08.009.
38. Lepaus BM, Rocha JS, São José J. 2020. Organic acids and hydrogen peroxide can replace chlorinated compounds as sanitizers on strawberries, cucumbers and rocket leaves. Food Sci Technol 40:242–249. https://doi.org/10.1590/fst.09519.
39. Ayebah B, Hung Y-C, Kim C, Frank JF. 2006. Efficacy of electrolyzed water in the inactivation of planktonic and biofilm *Listeria monocytogenes* in the presence of organic matter. J Food Prot 69:2143–2150. https://doi.org/10.4315/0362-028x-69.9.2143.
40. Zhao L, Poh CN, Wu J, Zhao X, He Y, Yang H. 2022. Effects of electrolysed water combined with ultrasound on inactivation kinetics and metabolite profiles of *Escherichia coli* biofilms on food contact surface. Innov Food Sci Emerg Technol 76:102917. https://doi.org/10.1016/j.ifset.2022.102917.
41. Yang H. 2012. PhD dissertation. Evaluating the antimicrobial mechanism of neutral electrochemically activated water on foodborne pathogens and their biofilms. University of Minnesota, Minneapolis, Minnesota.
42. Luu P, Chhetri VS, Janes ME, King JM, Adhikari A. 2021. Efficacy of gaseous chlorine dioxide in reducing *Salmonella enterica*, *E. coli* O157: H7, and *Listeria monocytogenes* on strawberries and blueberries. Lwt 141:110906. https://doi.org/10.1016/j.lwt.2021.110906.
43. Li K, Chiu Y-C, Jiang W, Jones L, Etienne X, Shen C. 2020. Comparing the efficacy of two triple-wash procedures with sodium hypochlorite, a lactic–citric acid blend, and a mix of peroxyacetic acid and hydrogen peroxide to inactivate *Salmonella*, *Listeria monocytogenes*, and Surrogate *Enterococcus faecium* on cucumbers and tomatoes. Front Sustain Food Syst 4:19. https://doi.org/10.3389/fsufs.2020.00019.
44. Pang X, Yuk H-G. 2019. Effects of the colonization sequence of *Listeria monocytogenes* and *Pseudomonas fluorescens* on survival of biofilm cells under food-related stresses and transfer to salmon. Food Microbiol 82:142–150. https://doi.org/10.1016/j.fm.2019.02.002.
45. Hartmann R, Jeckel H, Jelli E, Singh PK, Vaidya S, Bayer M, Rode DKH, Vidakovic L, Díaz-Pascual F, Fong JCN, Dragoš A, Lamprecht O, Thöming JG, Netter N, Häussler S, Nadell CD, Sourjik V, Kovács ÁT, Yildiz FH, Drescher K. 2021. Quantitative image analysis of microbial communities with BiofilmQ. Nat Microbiol 6:151–156. https://doi.org/10.1038/s41564-020-00817-4.
46. Rodríguez-Melcón C, Riesco-Peláez F, Carballo J, García-Fernández C, Capita R, Alonso-Calleja C. 2018. Structure and viability of 24-and 72-h-old biofilms formed by four pathogenic bacteria on polystyrene and glass contact surfaces. Food Microbiol 76:513–517. https://doi.org/10.1016/j.fm.2018.06.016.
47. Mahmud I, Kousik C, Hassell R, Chowdhury K, Boroujerdi AF. 2015. NMR spectroscopy identifies metabolites translocated from powdery mildew resistant rootstocks to susceptible watermelon scions. J Agric Food Chem 63:8083–8091. https://doi.org/10.1021/acs.jafc.5b02108.
48. Vong WC, Hua XY, Liu S-Q. 2018. Solid-state fermentation with *Rhizopus oligosporus* and *Yarrowia lipolytica* improved nutritional and flavour properties of okara. Lwt 90:316–322. https://doi.org/10.1016/j.lwt.2017.12.050.